

Domain-Wall Magnetoresistance in Antiferromagnetic Metals

Jun-Hui Zheng,¹ Arne Brataas,¹ Mathias Kläui,^{2,1} and Alireza Qaiumzadeh¹

¹*Center for Quantum Spintronics, Department of Physics,
Norwegian University of Science and Technology, NO-7491 Trondheim, Norway*
²*Institute for Physics, Johannes Gutenberg-University Mainz, 55128 Mainz, Germany*
(Dated: June 1, 2022)

Motivated by recent experiments, we theoretically study the domain-wall (DW) magnetoresistance (DWMR) in antiferromagnetic (AFM) metals. We compute the DWMR when the current is perpendicular to the wall for several different spin structures with various DW orientations. We find results for diffusive walls that are thicker than the mean free path and for thinner ballistic walls. In the diffusive transport regime, the DWs can enhance or unintuitively reduce the resistance, depending on the spin configuration along the DW orientation. Unlike ferromagnetic metals, the negative DWMR is caused neither by disorder nor by asymmetric spin-dependent scattering lifetimes. In the ballistic regime, the DWs enhance the resistance in a strongly anisotropic way originating from the DW orientation. This kind of intrinsic anisotropy depending on the spin ordering is a new feature in antiferromagnets in the absence of spin-orbit coupling.

Antiferromagnetic (AFM) materials are promising candidates in a new generation of spintronics devices [1, 2]. Controlling the motion of domain walls (DWs) is essential for data storage in magnetic memory devices [3]. The coupling between currents and spins enables efficient manipulation of AFM textures. Understanding this connection and the detection mechanisms for AFM textures is crucial in developing the frontier of the field further.

The interplay between charge or magnon currents and DWs in magnetically ordered materials has attracted intense interest in decades. The dynamics of ferromagnetic (FM) DWs and AFM-DWs have been studied in the presence of charge and magnon currents [4–27]. Besides, scatterings of charge and magnon currents from FM-DWs also have been explored extensively [28–38]. Recently, scattering of magnon currents from AFM-DWs [24–26, 39, 40] was studied. However, there is still no systematic study of charge current scatterings and associated DW magnetoresistance (DWMR) in AFM metals.

In FM metals, usually a DW acts as an effective barrier and increases the resistance [28–33]. Negative DWMR may appear in special cases when either the DW enhances electron decoherence in disordered systems [29] or the relaxation time is spin-dependent [41]. AFM systems, on the other hand, have more complex magnetic textures [42]. Consequently, the AFM-DWMR can exhibit more exotic properties [43]. A recent experimental study on the charge transport in the AFM metal Mn₂Au, showing anisotropic magnetoresistance and possibly effects of DWMR, has called for a theoretical understanding of AFM-DWMR [44, 45].

In this Letter, we theoretically study the resistance arising from DWs in AFM metals with a cubic crystal structure. Assuming that the DW is pinned sufficiently strongly, we focus on the charge transport perpendicular to a DW when the Fermi wavelength l_F is much smaller than the DW width w . We consider both diffusive regime when the mean free path (MFP) $l_{\text{MFP}} < w$ and ballistic

regime when $l_{\text{MFP}} \gtrsim w$ for different AFM spin structures.

In the diffusive regime, we find that the DWMR magnitude is $\propto 1/w$. However, in systems with parallel magnetic moment (PMM) and staggered magnetic moment (SMM) ordering along the current direction, the DWMR is positive and mostly negative, respectively. In the ballistic regime, it is positive and anisotropic. In the PMM configuration, the DWMR is $\propto 1/w^2$. While in the SMM configuration, it is $\propto 1/w$ for a moderate filling of the electron orbitals, and vanishes for a low or high filling.

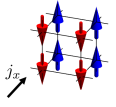
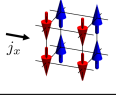
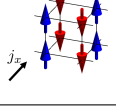
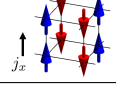
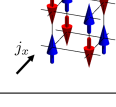
Model.—All AFM spin structures that we will treat are listed in Table I. We model the conduction electrons in these AFM metals with the Hamiltonian

$$\mathcal{H} = -J\mathbf{n} \cdot \boldsymbol{\sigma}\tau_z + h_1(\mathbf{k})\sigma_0\tau_x + h_2(\mathbf{k})\sigma_0\tau_0. \quad (1)$$

In above, \mathbf{k} is the electron wave vector. J denotes the s - d exchange interaction strength between the itinerant electrons and the staggered magnetization \mathbf{n} [46]. $\boldsymbol{\tau}$ and $\boldsymbol{\sigma}$ are the Pauli matrix vectors acting on the AFM sublattice space and the spin space, respectively. The structure factor $h_1(\mathbf{k}) = -t_1 \sum_{\mathbf{d}} \cos(\mathbf{k} \cdot \mathbf{d})$ describes hopping between the nearest-neighbor (NN) sites with antiparallel magnetic moments, and $h_2(\mathbf{k}) = -t_2 \sum_{\mathbf{b}} \cos(\mathbf{k} \cdot \mathbf{b})$ governs hopping between NN sites with PMMs, where the vector \mathbf{d} connects the NN A-B sites and \mathbf{b} connects the NN sublattices A-A or B-B. Note that for G -type AFM systems, there is no term h_2 . The Supplementary Material (SM) [47] describes the Hamiltonian (1) in more details. Without loss of generality, we consider $J > 0$, and set the lattice constant $a = 1$ and hopping integrals $t_1 = t_2 = t$ for simplicity.

Symmetry.—In a single AFM domain, \mathbf{n} is spatially independent. The system has a global $U(1) \times SU(2)$ symmetry. The $U(1)$ represents the charge conservation. The $SU(2)$ has generators $s_z = \mathbf{n} \cdot \boldsymbol{\sigma}$, $s_x\tau_x$, and $s_y\tau_x$, where \mathbf{s} are Pauli matrices that satisfy $s_i s_j = \delta_{ij} s_0 + i\epsilon_{ijk} s_k$. Next, we show that the symmetry reduces to $U(1) \times U(1)$ when DWs appear.

TABLE I. The DWMR for different AFM spin structures.

Spin structure ^a	Δ_{shift} and \mathbf{m}^* ($\hbar = a = 1$)	\mathcal{Z} for Eqs.(3) and (8)
 A_s	$\Delta_{\text{shift}} = -J^2/16\epsilon_a$ $m_x^* = \epsilon_a/2t^2$ $m_y^* = m_z^* = 1/2t$ $\epsilon_a = \sqrt{t^2 + J^2/4}$	$\mathcal{Z} = -\frac{J^2}{32t^2}$
 A_p	$\Delta_{\text{shift}} = tJ^2/16\epsilon_a^2$ $m_y^* = \epsilon_a/2t^2$ $m_x^* = m_z^* = 1/2t$	$\mathcal{Z} = \frac{J^2}{32\epsilon_a^2}$
 C_s	$\Delta_{\text{shift}} = -J^2/64\epsilon_c$ $m_x^* = m_y^* = \epsilon_c/2t^2$ $m_z^* = 1/2t$ $\epsilon_c = \sqrt{t^2 + J^2/16}$	$\mathcal{Z} = -\frac{J^2}{128t^2}$
 C_p	$\Delta_{\text{shift}} = tJ^2/64\epsilon_c^2$ $m_y^* = m_z^* = \epsilon_c/2t^2$ $m_x^* = 1/2t$	$\mathcal{Z} = \frac{J^2}{128\epsilon_c^2}$
 G	$\Delta_{\text{shift}} = -J^2/144\epsilon_g$ $m_x^* = m_y^* = m_z^* = \epsilon_g/2t^2$ $\epsilon_g = \sqrt{t^2 + J^2/36}$	$\mathcal{Z} = -\frac{J^2}{288t^2}$

^a The black vectors show the direction of the charge current along the x -direction. The DW is perpendicular to the x -axis.

Without loss of generality, we assume that the DW is perpendicular to the x -axis and set $\mathbf{n}(x) = (\sin\theta \cos\phi, \sin\theta \sin\phi, \cos\theta)$, where ϕ is constant and θ depends on x . In the first quantization theory, we replace the longitudinal wave-vector component k_x with the differential operator $-i\partial_x$ in Eq. (1). The transverse components k_y and k_z are good quantum numbers. We introduce a gauge transformation $\mathcal{R}_\theta = \exp[-i\phi\sigma_z/2] \exp[-i\theta\sigma_y/2]$, which makes the exchange term uniform, $\mathcal{R}_\theta^{-1}[\mathbf{n}(x) \cdot \boldsymbol{\sigma}] \mathcal{R}_\theta = \sigma_z$ [29]. After the transformation, the non-abelian gauge potential in the expression $\mathcal{R}_\theta^{-1}[-i\partial_x] \mathcal{R}_\theta = -i\partial_x - \lambda\sigma_y/2$ represents the DW, where $\lambda = d\theta/dx$ describes the spatial gradient of the spin texture. Further rotation transformation $\mathcal{T} = \exp[-i\sigma_x\pi/4] \exp[-i\tau_y\pi/4]$ separates the Hamiltonian into two decoupled 2×2 block matrices. The rotated Hamiltonian $\overline{\mathcal{H}} = \mathcal{T}^{-1} \mathcal{R}_\theta^{-1} \mathcal{H} \mathcal{R}_\theta \mathcal{T}$ becomes

$$\overline{\mathcal{H}} = J\sigma_y\tau_x + h_1(\hat{\mathbf{k}} + \hat{e}_x\lambda\sigma_z/2)\tau_z + h_2(\hat{\mathbf{k}} + \hat{e}_x\lambda\sigma_z/2), \quad (2)$$

where $\hat{e}_x = (1, 0, 0)$ and $\hat{\mathbf{k}} = (-i\partial_x, k_y, k_z)$. Eq. (2) has a global $U(1) \times U(1)$ symmetry. One $U(1)$ remains the charge conservation. The other one has the generator $\zeta = \sigma_z\tau_z$ that satisfies $[\zeta, \overline{\mathcal{H}}] = 0$, corresponding to an effective spin conservation. The quantum states decouple into eigenstates with $\zeta = 1$ and $\zeta = -1$. In the following, we compute the AFM-DWMR based on the effective electronic Hamiltonian Eq. (2).

Diffusive transport theory.—When the MFP is significantly shorter than the DW width w , electrons move diffusively. The corresponding FM-DWMR has previously

been evaluated using perturbative quantum field theory (QFT) [29, 33] or Boltzmann transport equation [30]. To circumvent the complicated evaluation of Feynman diagrams in QFT, we provide a new and considerably simpler method for computing the diffusive transport in AFM systems when the DW is wide $w > l_F$ and $\lambda(x)$ varies slowly.

We divide the DW into small spin-spiral (SS) domains and treat the gradient $\lambda(x)$ in each SS domain spatially independently. In the diffusive regime, Ohm's law applies. The resistance for each effective spin direction $\zeta = \pm 1$ is a series resistance, $R_\zeta = \int_{-L/2}^{L/2} [1/\sigma_\zeta(\lambda)] dx/S$, where $\sigma_\zeta(\lambda)$ is the conductivity in a SS domain. L is the system length along the x -axis and S is the cross-section. In determining the transport, the two effective spin directions function as parallel circuits. The total resistance R is determined by $1/R = 1/R_+ + 1/R_-$. The DWMR is $R_w = R - R_0 \simeq -\sigma_0^{-2} S^{-1} \int_{-L/2}^{L/2} \delta\sigma dx$, where $R_0 = L/S\sigma_0$ is the resistance of a single AFM domain. $\sigma_0 = 2\sigma_+(0) = 2\sigma_-(0)$ is the conductivity for a single domain since transport is spin degenerate in diffusive AFMs. $\delta\sigma(\lambda) = \sigma(\lambda) - \sigma_0$ is the correction arising from SS and $\sigma(\lambda) = \sigma_+(\lambda) + \sigma_-(\lambda)$.

At low filling regime that only the low energy states in the lowest band of $\overline{\mathcal{H}}(\lambda)$ are occupied, the eigenenergies E_ζ^s for a SS domain (where s denotes different energy levels for each ζ) [47] becomes especially simple, $E \simeq c\lambda^2 + 2b\lambda k_x + k_x^2/2m_x^* + k_y^2/2m_y^* + k_z^2/2m_z^* + \text{const.}$, where \mathbf{m}^* is the effective mass. The Drude conductivity is $\sigma(\lambda) = e^2 n \tau / |m_x^*|$, where $n = k_F^x k_F^y k_F^z / 3\pi^2$ is the electron density, k_F^i is the anisotropic Fermi wavevector for $i = x, y, z$, and τ is the electron lifetime. SS contributes an energy shift $\delta E = \Delta_{\text{shift}} \lambda^2$, where $\Delta_{\text{shift}} = c - 2b^2 m_x^*$. The relative change in the resistance due to the DW is

$$\frac{R_w}{R_0} = 2^{\pm 1} \cdot \frac{(l_F^x)^2}{Lw} \cdot 3\mathcal{Z}, \quad (3)$$

where the dimensionless quantity $\mathcal{Z} = m_x^* \Delta_{\text{shift}}$ is a function of J^2/t^2 , $l_F^i = 1/k_F^i$ is the anisotropic Fermi wavelength, and $2^{\pm 1}$ refers to 180° and 90° DWs, respectively. We have assumed that for a 180° DW, the staggered texture is $\cos\theta = \tanh(x/w)$ [24, 25], and for a 90° DW, $\cos 2\theta = \tanh(x/w)$. Thus, $\int_{-L/2}^{L/2} \lambda^2 dx = 2/w$ and $1/2w$, and $\lambda_{\text{max}} = 1/w$ and $1/2w$ for these DWs, respectively.

Table I lists the effective mass \mathbf{m}^* , the energy shift coefficient Δ_{shift} , and the parameter \mathcal{Z} for each type. The DWMR in A_p - and C_p -type AFM are positive. In strong contrast, it is negative in A_s -, C_s - and G -type AFM due to negative \mathcal{Z} caused by negative energy shift. In fact, from Drude's formula, negative energy shift enhances the electron density and thus induces a negative DWMR. Note that for these three types, the magnetic moments are staggered along the current direction (which is perpendicular to the DW). Table I shows that the coefficient \mathcal{Z} is larger and thus the DW effect is stronger for

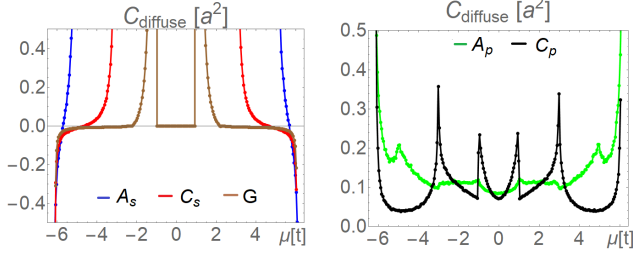


FIG. 1. The coefficient C_{diffuse} with respect to the chemical potential μ for different cases. $J = t$.

a larger exchange interaction J . As compared to A_s and C_s types, the DW effect in G type is suppressed because of a smaller $|\mathcal{Z}|$. We attribute it to a larger magnetic self-screening effect in G -type AFM spin structure.

In general, still considering the diffusive regime, using the Kubo formula [47, 48], the electric conductivity for a SS domain with constant gradient λ is

$$\sigma_{\zeta}(\lambda) = e^2\tau \sum_s \int_{\text{BZ}} \frac{d^3\mathbf{k}}{(2\pi)^3} (v_x^{\zeta s})^2 \delta(E_{\zeta}^s - \mu), \quad (4)$$

where $v_x^{\zeta s} = \partial E_{\zeta}^s / \partial k_x$ is the group velocity. By expanding Eq. (4) as a function of the gradient λ , the correction from SS is of the order of λ^2 . The relative DWMR for a 180° DW and a 90° DW, respectively, becomes

$$\frac{R_w}{R_0} = 2 \pm 1 \frac{C_{\text{diffuse}}}{Lw}, \quad (5)$$

where

$$C_{\text{diffuse}} = -\frac{e^2\tau}{\sigma_0} \sum_{\zeta,s} \int_{\text{BZ}} \frac{d^3\mathbf{k}}{(2\pi)^3} \mathcal{F}_2[E_{\zeta}^s] \delta(E_{\zeta}^s|_{\lambda=0} - \mu), \quad (6)$$

and $\mathcal{F}_2[E] = [\ddot{E}'E'/2 - \dot{E}\dot{E}'' - \ddot{E}E''/2 + E''' \dot{E}^2/2E' - E''^2 \dot{E}^2/2E'^2 + E'' \dot{E}\dot{E}'/E']|_{\lambda=0}$ [47]. We have used the convention that $\dot{E} = \partial_{\lambda} E$ and $E' = \partial_{k_x} E$. Eq. (5) demonstrates that in the diffusive transport regime, the DWMR is inversely proportional to the DW width.

At low filling, Eq. (5) is consistent with Eq. (3). From Eq. (4), a negative energy shift from SS decreases the resistance because both the density of state (DOS) and the Fermi velocity are enhanced at the Fermi level μ .

In Fig. 1, we show the numerical results of the coefficient C_{diffuse} , by employing Monte Carlo method for the integrals in Eq. (6). The results confirm the existence of negative DWMR in A_s -, C_s - and G -type AFM at the low or high filling case. The coefficient (6) diverges and therefore the expansion breaks down when the chemical potential $\mu \in [-4t - J, 4t + J]$ in the A_s model, $\mu \in [-2t - J, 2t + J]$ in the C_s model, or $\mu \simeq \pm J$ in the G model, in which region the velocity $E' = v_x$ can be zero and the DOS is not a differentiable function of λ anymore [47].

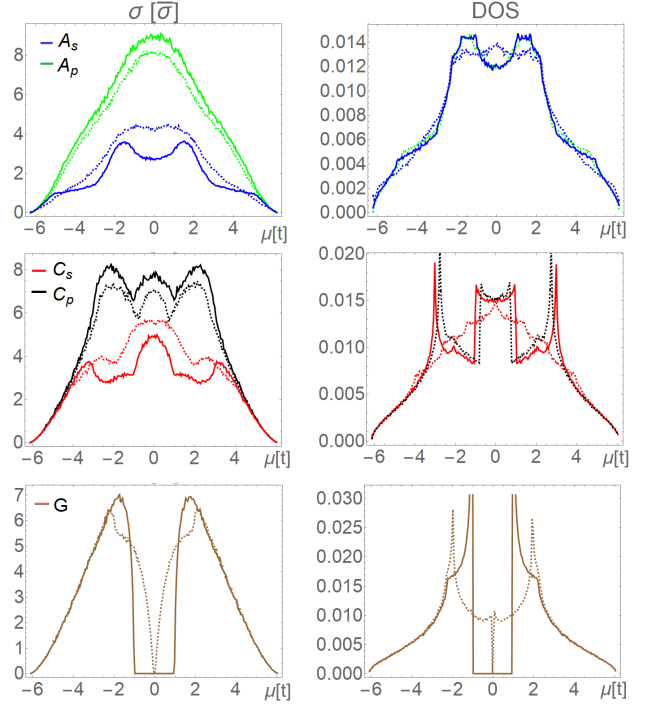


FIG. 2. Diffuse conductivity $\sigma(\lambda)$ and DOS as functions of the chemical potential μ . For visualization the difference in different SS cases (solid lines are for $\lambda = 0$ and dotted lines are for $\lambda = 1/a$), we chose a large exchange interaction, $J = t$, and a large $\lambda = 1/a$. The result for $\lambda = 1/2a$ can be found in supplementary [47]. The unit $\bar{\sigma} = e^2\tau/3\pi^2 m_0 a^3$, where $m_0 = 1/2t$. The DOS at $\lambda = 0$ is same for A_s and A_p , and also for C_s and C_p .

To understand the DWMR in all regions, in Fig. 2, we plot the SS conductivity and DOS for $\lambda = 0$ and $\lambda = 1/a$ (the spiral period is $2\pi/\lambda$), respectively. Comparing A_s - and A_p -types, or C_s - and C_p -types, we find that the single domain conductivity ($\lambda = 0$) along the PMM direction is larger than that along the SMM direction. It means that along the SMM direction, the electron mobility is suppressed according to Eq. (4). Especially for a low filling, along the SMM direction, the system has a larger effective mass, suppressing the electron velocity and conductivity σ_0 . The anisotropic mass may explain the observed anisotropic magnetoresistance in Mn_2Au [44, 45].

Along the PMM direction, spin spiral always decreases the conductivity and thus the DWMR is positive. In contrast, along the SMM direction, SS usually increases the conductivity, leading to a negative DWMR. An interpretation is that SS or DW effectively eases the magnetic staggering and thus enhances the electron mobility. In particular, for the A_s -type at $\mu \simeq 0$, neglecting the correction of DOS from spin-spiral λ and taking only the velocity corrections into account, we estimate $\delta\sigma(\lambda)/\sigma_0 = \mathcal{A} \cdot a^2 \lambda^2$, where $\mathcal{A} = Jt^2/4\epsilon_a(2t^2 + J^2 - 2\epsilon_a J)$ and $\epsilon_a = \sqrt{t^2 + J^2}/4$. The estimated correction for the conduc-

tivity from SS is positive and qualitatively matches our numerical results (for $J = t$, $\mathcal{A} \sim 1/4$). The relative DWMR is $R_w/R_0 = -2^{\pm 1} \cdot (a^2/Lw) \cdot \mathcal{A} < 0$. There is some small energy regions for the A_s , C_s and G model, SS decreases the conductivity and the coefficient $\mathcal{C}_{\text{diffuse}}$ becomes positive (see Fig. 1). In these regions, the conducting channels are (strongly) suppressed due to SS, which can be observed in the DOS in Fig. 2.

In experiments, to check such DW effects, one could measure the magnetoresistance for single crystalline samples with and without DWs along different crystallographic directions.

Ballistic transport theory.—When the electron MFP is larger than the DW width, the conductance along the x -direction at zero temperature reads

$$G = e^2 S \sum_{\zeta_s} \int_{\text{BZ}}^{v_x^{\zeta_s} > 0} \frac{d^3 \mathbf{k}}{(2\pi)^3} v_x^{\zeta_s} |_{\lambda=0} T_{\zeta_s, k_x} \delta(E_{\zeta}^s |_{\lambda=0} - \mu), \quad (7)$$

where T_{ζ_s, k_x} is the transmission coefficient for each channel [49]. The integral region is confined to $v_x^{\zeta_s} > 0$ for the right moving electrons. Since λ varies slowly, the adiabatic approximation can be applied. In other words, we can treat the quasiparticle motion classically [50]. The transmission coefficient $T_{k_x} = 1$ for open channels and $T_{k_x} = 0$ for closed channels. The DWMR is determined by the number of open channels in a single domain that become closed due to the DW, analogous to the calculation for FM metals. The maximum value of the gradient of the spin structure, λ_{max} , determines the reduced number of channels. Since the number of channels is reduced, the ballistic DWMR is positive.

When the filling is low, $R_0 = (4\pi^2 \hbar / e^2) (l_F^y l_F^z / S)$. For A_s , C_s , and G -types, DWs are transparent and cause no additional resistance, since all low energy channels are open due to the negative energy shift $\delta E = \Delta_{\text{shift}} \lambda_{\text{max}}^2$. For A_p and C_p -types, δE is positive and we obtain

$$\frac{R_w}{R_0} = \frac{(l_F^x)^2}{4^d w^2} \cdot 2Z, \quad (8)$$

where $d = 0$ for a 180° DW and $d = 1$ for a 90° DW. In the case of a high filling, the results are the same.

The situation differs in the moderate filling case. Specially for the A_s -type case, the local SS dispersion is $E_{\zeta}^s = h_2 + \mathcal{E}_{\zeta}^s$, where $h_2 = -2t(\cos k_y + \cos k_z)$ and $\mathcal{E}_{\zeta}^{\pm} = 2\zeta t \sin(\lambda/2) \sin k_x \pm \sqrt{4t^2 \cos^2(\lambda/2) \cos^2 k_x + J^2}$. Rewriting $\mathcal{E}_{\zeta}^{\pm}(\lambda(x)) = \mathcal{E}_{\zeta}^{\pm}(\lambda = 0) + V_{\text{eff}}$, we find that back scattering exists near $k_x = \pm\pi/2$, where the effective potential $V_{\text{eff}} = \pm 2t \sin[\lambda(x)/2]$. For a wide DW $w \gg a$, we have $\text{Max}[|V_{\text{eff}}|] = ta/2^d w$ for 180° and 90° DWs. Furthermore, we obtain the relative DWMR

$$\frac{R_w}{R_0} = -\frac{\delta G}{G_0} = \mathcal{C}_{A_s} \cdot \frac{a}{2^d w}, \quad (9)$$

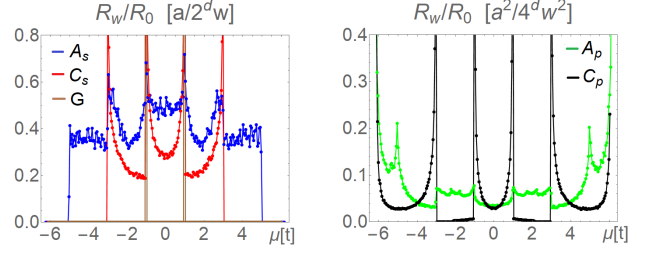


FIG. 3. R_w/R_0 as functions of the chemical potential. $J = t$.

where $\mathcal{C}_{A_s}(\mu) = t(\rho_{\mu-J}^{2D} + \rho_{\mu+J}^{2D})/2 \int_{J < |\epsilon - \mu| < 2\epsilon_a} \rho_{\epsilon}^{2D} d\epsilon$ and ρ_{ϵ}^{2D} is the two-dimensional DOS of h_2 [47]. By assuming that ρ_{ϵ}^{2D} is uniform for $\epsilon \in [-4t, 4t]$, we estimate that $\mathcal{C}_{A_s} \sim t/2(2\epsilon_a - J)$ for the moderate filling case and obtain $\mathcal{C}_{A_s} = 0$ for $\mu \notin [-4t - J, 4t + J]$ [47]. This estimation fits pretty good with numerical results. For instant, $J = t$, we get $\mathcal{C}_{A_s} \sim 0.4$ at a moderate filling, close to the numerical result shown in Fig. 3. For the A_p -type, back scattering exists near $k_x = 0$ due to the positive energy shift $\delta E \propto \lambda_{\text{max}}^2$. Detailed discussion shows

$$\frac{R_w}{R_0} = \mathcal{D}_{A_p} \cdot \frac{a^2}{4^d w^2}, \quad (10)$$

and the coefficient is estimated to be $\mathcal{D}_{A_p} \sim J/16\epsilon_a$ [47]. For $J = 1$, $\mathcal{D}_{A_p} \simeq 0.056$, which also well agrees with the numerical result. The dependence of the DWMR on the DW width in the A_p -type is the same as in FM metals, but differently, it is strongly suppressed through the ratio J/t [32, 33, 47]. C_s -type has similar behavior with the A_s -type. We plot the relative DWMR R_w/R_0 in Fig. 3. For A_s -type and C_s -type, the DWMR is $\propto a/w$ for a moderate filling and vanishes for a low or high filling. In contrast, for the A_p -type and C_p -type, the DW resistance is $\propto a^2/w^2$ for a moderate filling, and $\propto (l_F^x)^2/w^2$ for a low or high filling. For G -type, DW resistance is nonzero only for $\mu \simeq \pm J$, where backscattering happens. More details can be found in SM [47].

The qualitative dependence of the DWMR on the DW properties, such as the width, might be measurable in experiments. By varying the anisotropy of the systems, for example by strain, one can vary the width and ascertain the DWMR in conjunction with magnetic imaging using x-ray magnetic linear dichroism contrast [39, 44].

Conclusions.—We have systemically studied the DWMR in AFM metals. The behavior of the DWMR in AFMs is richer and offers more tunability than in ferromagnets. The DWMR depends on the orientation of the DW as well as on the AFM structure. In contrast to FM-DW, the AFM DWMR can be negative even in the diffusive regime with a spin-independent relaxation time.

This work has been supported by the European Research Council via Advanced Grant No. 669442 “Insulatronics”, the Research Council of Norway through

its Centres of Excellence funding scheme, Project No. 262633, “QuSpin”, and the German Research Foundation (SFB TRR 173 Spin+X, projects A01 and B02). The authors thank O. Gomonay and M. Jourdan for discussions.

-
- [1] V. Baltz, A. Manchon, M. Tsoi, T. Moriyama, T. Ono, and Y. Tserkovnyak, *Rev. Mod. Phys.* **90**, 015005 (2018).
- [2] R. Lebrun, A. Ross, S. A. Bender, A. Qaiumzadeh, L. Baldrati, J. Cramer, A. Brataas, R. A. Duine, and M. Kläui, *Nature (London)* **561**, 222 (2018).
- [3] M. Foerster, O. Boule, S. Esefelder, R. Mattheis, and M. Kläui, “Domain wall memory device,” in *Handbook of Spintronics*, edited by Y. Xu, D. D. Awschalom, and J. Nitta (Springer Netherlands, Dordrecht, 2014) pp. 1–46.
- [4] L. Berger, *Journal of Applied Physics* **55**, 1954 (1984).
- [5] G. Tatara and H. Kohno, *Phys. Rev. Lett.* **92**, 086601 (2004).
- [6] S. Zhang and Z. Li, *Phys. Rev. Lett.* **93**, 127204 (2004).
- [7] A. Thiaville, Y. Nakatani, J. Miltat, and Y. Suzuki, *Europhysics Letters (EPL)* **69**, 990 (2005).
- [8] G. Tatara, T. Takayama, H. Kohno, J. Shibata, Y. Nakatani, and H. Fukuyama, *Journal of the Physical Society of Japan* **75**, 064708 (2006), <https://doi.org/10.1143/JPSJ.75.064708>.
- [9] A. Mougín, M. Cormier, J. P. Adam, P. J. Metaxas, and J. Ferré, *Europhysics Letters (EPL)* **78**, 57007 (2007).
- [10] S.-W. Jung, W. Kim, T.-D. Lee, K.-J. Lee, and H.-W. Lee, *Applied Physics Letters* **92**, 202508 (2008), [arXiv:0804.3864 \[cond-mat.mes-hall\]](https://arxiv.org/abs/0804.3864).
- [11] G. Tatara, H. Kohno, and J. Shibata, *Physics Reports* **468**, 213 (2008).
- [12] J. Ryu, S.-B. Choe, and H.-W. Lee, *Phys. Rev. B* **84**, 075469 (2011).
- [13] C. H. Marrows, *Advances in Physics* **54**, 585 (2005), <https://doi.org/10.1080/00018730500442209>.
- [14] O. Boule, G. Malinowski, and M. Klui, *Materials Science and Engineering: R: Reports* **72**, 159 (2011).
- [15] M. Yamanouchi, D. Chiba, F. Matsukura, and H. Ohno, *Nature* **428**, 539 (2004).
- [16] M. Yamanouchi, D. Chiba, F. Matsukura, T. Dietl, and H. Ohno, *Phys. Rev. Lett.* **96**, 096601 (2006).
- [17] M. Yamanouchi, J. Ieda, F. Matsukura, S. E. Barnes, S. Maekawa, and H. Ohno, *Science* **317**, 1726 (2007), <https://science.sciencemag.org/content/317/5845/1726.full.pdf>.
- [18] K.-J. Kim, J. Ryu, G.-H. Gim, J.-C. Lee, K.-H. Shin, H.-W. Lee, and S.-B. Choe, *Phys. Rev. Lett.* **107**, 217205 (2011).
- [19] D. Hinzke and U. Nowak, *Phys. Rev. Lett.* **107**, 027205 (2011).
- [20] T. Shiino, S.-H. Oh, P. M. Haney, S.-W. Lee, G. Go, B.-G. Park, and K.-J. Lee, *Phys. Rev. Lett.* **117**, 087203 (2016).
- [21] O. Gomonay, T. Jungwirth, and J. Sinova, *Phys. Rev. Lett.* **117**, 017202 (2016).
- [22] A. C. Swaving and R. A. Duine, *Journal of Physics: Condensed Matter* **24**, 024223 (2011).
- [23] E. G. Tveten, A. Qaiumzadeh, O. A. Tretiakov, and A. Brataas, *Phys. Rev. Lett.* **110**, 127208 (2013).
- [24] A. Qaiumzadeh, L. A. Kristiansen, and A. Brataas, *Phys. Rev. B* **97**, 020402 (2018).
- [25] E. G. Tveten, A. Qaiumzadeh, and A. Brataas, *Phys. Rev. Lett.* **112**, 147204 (2014).
- [26] S. K. Kim, Y. Tserkovnyak, and O. Tchernyshyov, *Phys. Rev. B* **90**, 104406 (2014).
- [27] H.-J. Park, Y. Jeong, S.-H. Oh, G. Go, J. H. Oh, K.-W. Kim, H.-W. Lee, and K.-J. Lee, *arXiv e-prints*, [arXiv:2001.07351](https://arxiv.org/abs/2001.07351) (2020), [arXiv:2001.07351 \[cond-mat.mes-hall\]](https://arxiv.org/abs/2001.07351).
- [28] G. G. Cabrera and L. M. Falicov, *physica status solidi (b)* **61**, 539 (1974), <https://onlinelibrary.wiley.com/doi/pdf/10.1002/pssb.2220610219>.
- [29] G. Tatara and H. Fukuyama, *Phys. Rev. Lett.* **78**, 3773 (1997).
- [30] P. M. Levy and S. Zhang, *Phys. Rev. Lett.* **79**, 5110 (1997).
- [31] Y. Lyanda-Geller, I. L. Aleiner, and P. M. Goldbart, *Phys. Rev. Lett.* **81**, 3215 (1998).
- [32] J. B. A. N. van Hoof, K. M. Schep, A. Brataas, G. E. W. Bauer, and P. J. Kelly, *Phys. Rev. B* **59**, 138 (1999).
- [33] A. Brataas, G. Tatara, and G. E. W. Bauer, *Phys. Rev. B* **60**, 3406 (1999).
- [34] U. Ebels, A. Radulescu, Y. Henry, L. Piraux, and K. Ounadjela, *Phys. Rev. Lett.* **84**, 983 (2000).
- [35] E. Šimánek, *Phys. Rev. B* **63**, 224412 (2001).
- [36] A. D. Kent, J. Yu, U. Rüdiger, and S. S. P. Parkin, *Journal of Physics Condensed Matter* **13**, R461 (2001).
- [37] P. Yan and G. E. W. Bauer, *Phys. Rev. Lett.* **109**, 087202 (2012).
- [38] A. von Bieren, A. K. Patra, S. Krzyk, J. Rhensius, R. M. Reeve, L. J. Heyderman, R. Hoffmann-Vogel, and M. Kläui, *Phys. Rev. Lett.* **110**, 067203 (2013).
- [39] A. Ross, R. Lebrun, O. Gomonay, D. A. Grave, A. Kay, L. Baldrati, S. Becker, A. Qaiumzadeh, C. Ulloa, G. Jakob, F. Kronast, J. Sinova, R. Duine, A. Brataas, A. Rothschild, and M. Kläui, *Nano Lett.* **20**, 306 (2020), [arXiv:1907.02751 \[cond-mat.mtrl-sci\]](https://arxiv.org/abs/1907.02751).
- [40] P. Shen, Y. Tserkovnyak, and S. K. Kim, *arXiv e-prints*, [arXiv:2002.11777](https://arxiv.org/abs/2002.11777) (2020), [arXiv:2002.11777 \[cond-mat.mes-hall\]](https://arxiv.org/abs/2002.11777).
- [41] R. P. van Gorkom, A. Brataas, and G. E. W. Bauer, *Phys. Rev. Lett.* **83**, 4401 (1999).
- [42] J. Lan, W. Yu, and J. Xiao, *Nature Communications* **8**, 178 (2017), [arXiv:1706.01617 \[cond-mat.other\]](https://arxiv.org/abs/1706.01617).
- [43] R. Jaramillo, T. F. Rosenbaum, E. D. Isaacs, O. G. Shpyrko, P. G. Evans, G. Aeppli, and Z. Cai, *Phys. Rev. Lett.* **98**, 117206 (2007).
- [44] S. Y. Bodnar, Y. Skourski, S. P. Bommanaboyena, M. Kläui, and M. Jourdan, *arXiv e-prints*, [arXiv:1909.12606](https://arxiv.org/abs/1909.12606) (2019), [arXiv:1909.12606 \[cond-mat.mtrl-sci\]](https://arxiv.org/abs/1909.12606).
- [45] S. Y. Bodnar, L. Šmejkal, I. Turek, T. Jungwirth, O. Gomonay, J. Sinova, A. A. Sapozhnik, H. J. Elmers, M. Kläui, and M. Jourdan, *Nature Communications* **9**, 348 (2018), [arXiv:1706.02482 \[cond-mat.mtrl-sci\]](https://arxiv.org/abs/1706.02482).
- [46] R. Cheng and Q. Niu, *Phys. Rev. B* **86**, 245118 (2012).
- [47] J.-H. Zheng, A. Qaiumzadeh, and A. Brataas, *Supplementary* (2020).
- [48] G. D. Mahan, *Many Particle Physics, Third Edition* (Plenum, New York, 2000).
- [49] Y. V. Nazarov and Y. M. Blanter, *Quantum Transport: Introduction to Nanoscience* (Cambridge University Press, 2009).

- [50] In this case, the motion of the quasiparticle is governed by Hamilton's equations, $\dot{x} = \partial_{k_x} E_\zeta^s(k_x, \lambda(x))$ and $\dot{k}_x = -\partial_x E_\zeta^s(k_x, \lambda(x))$, where $\dot{x} = v_x^{\zeta^s}$ is the group velocity. k_y and k_z are good quantum numbers, and they are hidden in above expressions.
- [51] B. A. Bernevig and T. L. Hughes, *Topological Insulators and Topological Superconductors*, stu - student edition ed. (Princeton University Press, 2013).

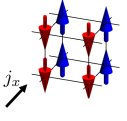
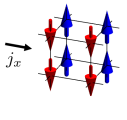
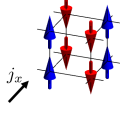
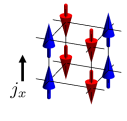
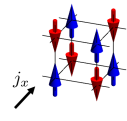
CONTENTS

Acknowledgments	4
References	5
Supplementary	7
Hamiltonian and spin-spiral spectrum	7
Charge conductivity in the spin-spiral system	7
Order by order expansion of Eq.(4) in main text	9
Ballistic transport	10
Ballistic transport for ferromagnetic metals	11
Fig. 5: Plot of diffuse conductivity $\sigma(\lambda)$ and DOS	12
Fig. 6: Plot of ballistic conductance G_0	12

SUPPLEMENTARY

Hamiltonian and spin-spiral spectrum

TABLE II. Hamiltonian, spin-spiral spectrum and parameters for different AFM spin structure

Spin structure ^a	Hamiltonian $\mathcal{H} = -J\mathbf{n} \cdot \boldsymbol{\sigma}\tau_z + h_1(\mathbf{k})\sigma_0\tau_x + h_2(\mathbf{k})\sigma_0\tau_0$ Spin-spiral spectrum E_{ζ}^s , where $s = \pm 1$ and $\zeta = \pm 1$	Δ_{shift} and \mathbf{m}^* ($\hbar = a = 1$)	Coefficient \mathcal{Z}
 A_s	$h_1 = -2t \cos k_x$ $h_2 = -2t(\cos k_y + \cos k_z)$ $E_{\zeta}^s = h_2 + \mathcal{E}_{\zeta}^s$ $\mathcal{E}_{\zeta}^s = 2\zeta t \sin \frac{\lambda}{2} \sin k_x + s\sqrt{4t^2 \cos^2 \frac{\lambda}{2} \cos^2 k_x + J^2}$	$\Delta_{\text{shift}} = -J^2/16\epsilon_a$ $m_x^* = \epsilon_a/2t^2$ $m_y^* = m_z^* = 1/2t$ $\epsilon_a = \sqrt{t^2 + J^2/4}$	$\mathcal{Z} = -\frac{J^2}{32t^2}$
 A_p	$h_1 = -2t \cos k_y$ $h_2 = -2t(\cos k_x + \cos k_z)$ $E_{\zeta}^s = -2t \cos \frac{\lambda}{2} \cos k_x - 2t \cos k_z$ $+ s\sqrt{4t^2(\cos k_y - \zeta \sin \frac{\lambda}{2} \sin k_x)^2 + J^2}$	$\Delta_{\text{shift}} = tJ^2/16\epsilon_a^2$ $m_y^* = \epsilon_a/2t^2$ $m_x^* = m_z^* = 1/2t$	$\mathcal{Z} = \frac{J^2}{32\epsilon_a^2}$
 C_s	$h_1 = -2t(\cos k_x + \cos k_y)$ $h_2 = -2t \cos k_z$ $E_{\zeta}^s = -2t \cos k_z + 2\zeta t \sin \frac{\lambda}{2} \sin k_x$ $+ s\sqrt{4t^2[\cos \frac{\lambda}{2} \cos k_x + \cos k_y]^2 + J^2}$	$\Delta_{\text{shift}} = -J^2/64\epsilon_c$ $m_x^* = m_y^* = \epsilon_c/2t^2$ $m_z^* = 1/2t$ $\epsilon_c = \sqrt{t^2 + J^2/16}$	$\mathcal{Z} = -\frac{J^2}{128t^2}$
 C_p	$h_1 = -2t(\cos k_y + \cos k_z)$ $h_2 = -2t \cos k_x$ $E_{\zeta}^s = -2t \cos \frac{\lambda}{2} \cos k_x$ $+ s\sqrt{4t^2(\cos k_y + \cos k_z - \zeta \sin \frac{\lambda}{2} \sin k_x)^2 + J^2}$	$\Delta_{\text{shift}} = tJ^2/64\epsilon_c^2$ $m_y^* = m_z^* = \epsilon_c/2t^2$ $m_x^* = 1/2t$	$\mathcal{Z} = \frac{J^2}{128\epsilon_c^2}$
 G	$h_1 = -2t(\cos k_x + \cos k_y + \cos k_z)$ $h_2 = 0$ $E_{\zeta}^s = 2\zeta t \sin \frac{\lambda}{2} \sin k_x$ $+ s\sqrt{4t^2[\cos \frac{\lambda}{2} \cos k_x + \cos k_y + \cos k_z]^2 + J^2}$	$\Delta_{\text{shift}} = -J^2/144\epsilon_g$ $m_x^* = m_y^* = m_z^*$ $= \epsilon_g/2t^2$ $\epsilon_g = \sqrt{t^2 + J^2/36}$	$\mathcal{Z} = -\frac{J^2}{288t^2}$

^a The black vectors show the direction of the charge current along the x -direction. The DW is perpendicular to the x -axis.

Charge conductivity in the spin-spiral system

We rewrite the Hamiltonian as $\mathcal{H} = \mathcal{H}_0(\mathbf{k}) + V(x)$, where $\mathcal{H}_0(\mathbf{k}) = h_1(\mathbf{k})\sigma_0\tau_x + h_2(\mathbf{k})\sigma_0\tau_0$ contains all hopping terms and $V(x) = -J\mathbf{n}(x) \cdot \boldsymbol{\sigma}\tau_z$ represents the effective potential. The matrix representation of the current corresponding

to the U(1) charge conservation is $\mathcal{J}_{\mathbf{k}} = \partial_{k_x} \mathcal{H}_0(\mathbf{k})$ [51]. We have set $e = 1$ and $\hbar = 1$ for simplicity. The gauge transformation $\mathcal{R}_\theta \mathcal{T} = \exp[-i\phi\sigma_z/2] \exp[-i\theta\sigma_y/2] \exp[-i\sigma_x\pi/4] \exp[-i\tau_y\pi/4]$ gives $\overline{\mathcal{H}} = \mathcal{T}^{-1} \mathcal{R}_\theta^{-1} \mathcal{H} \mathcal{R}_\theta \mathcal{T} = \overline{\mathcal{H}}_0 + \overline{V}$, where $\overline{\mathcal{H}}_0 = h_1(\hat{\mathbf{k}} + \hat{e}_x \lambda \sigma_z/2) \tau_z + h_2(\hat{\mathbf{k}} + \hat{e}_x \lambda \sigma_z/2)$ and $\overline{V} = J \sigma_y \tau_x$. For the spin-spiral case that λ is a constant, the wave vector k_x becomes a good quantum number and the current matrix after the gauge transformation becomes,

$$\overline{\mathcal{J}}_{\mathbf{k}} = \mathcal{T}^{-1} \mathcal{R}_\theta^{-1} \mathcal{J}_{\mathbf{k}} \mathcal{R}_\theta \mathcal{T} = \partial_{k_x} \overline{\mathcal{H}}_0 = \partial_{k_x} \overline{\mathcal{H}}. \quad (11)$$

The second quantization form of the Hamiltonian, can be written in the following form

$$\hat{H} = \sum_{\mathbf{k}, s, s'} \hat{c}_{\mathbf{k}, s}^\dagger \overline{\mathcal{H}}_{\mathbf{k}; s, s'} \hat{c}_{\mathbf{k}, s'}, \quad (12)$$

where $\hat{c}_{\mathbf{k}}$ is the Fourier transformed of the rotated annihilation operator $\hat{c}_{\mathbf{x}} = \mathcal{T}^{-1} \mathcal{R}_\theta^{-1} \hat{c}_{\mathbf{x}}^0$ and $\hat{c}_{\mathbf{x}}^0$ is the original annihilation operator. Since ζ is a conserved spin in our systems and we focus on each subspace with $\zeta = 1$ or $\zeta = -1$, we have omitted the notation ζ for simplicity. The current operator is

$$\hat{j}_x = \sum_{\mathbf{k}, s, s'} \hat{c}_{\mathbf{k}, s}^\dagger \overline{\mathcal{J}}_{\mathbf{k}; s, s'} \hat{c}_{\mathbf{k}, s'}. \quad (13)$$

We will further write these operators in the eigen-basis of the Hamiltonian $\overline{\mathcal{H}}$. We introduce a unitary transformation $U_{\mathbf{k}}$ so that $\overline{\mathcal{H}}_{\mathbf{k}} = U_{\mathbf{k}}^\dagger \Lambda_{\mathbf{k}} U_{\mathbf{k}}$, where the matrix $\Lambda_{\mathbf{k}} = \text{diag}\{E^+(\mathbf{k}), E^-(\mathbf{k})\}$ is diagonal. The current operator becomes

$$\hat{j}_x = \sum_{\mathbf{k}, s, s'} \hat{d}_{\mathbf{k}, s}^\dagger J_{\mathbf{k}; s, s'} \hat{d}_{\mathbf{k}, s'}, \quad (14)$$

where $\hat{d}_{\mathbf{k}} = U_{\mathbf{k}} \hat{c}_{\mathbf{k}}$ is the annihilation operator corresponding to the eigen-basis and $J_{\mathbf{k}} = U_{\mathbf{k}} \overline{\mathcal{J}}_{\mathbf{k}} U_{\mathbf{k}}^\dagger$.

The conductivity in Kubo formula is [48]

$$\sigma = \lim_{\omega \rightarrow 0} \left\{ \frac{\text{Im}[\pi(i\omega_n \rightarrow \omega + i\delta)]}{\omega} \right\}, \quad (15)$$

where the current-current correlation is

$$\begin{aligned} \pi(i\omega_n) &= \frac{1}{V} \int_0^\beta dt e^{i\omega_n t} \langle T_t \hat{j}_x(t) \hat{j}_x(0) \rangle \\ &= \frac{1}{\beta} \sum_{ip} \int \frac{d^3 \mathbf{k}}{(2\pi)^3} \text{Tr} [J_{\mathbf{k}} \mathcal{G}_{\mathbf{k}}(ip + i\omega) J_{\mathbf{k}} \mathcal{G}_{\mathbf{k}}(ip)]. \end{aligned} \quad (16)$$

Here $\mathcal{G}_{\mathbf{k}}(ip)$ is diagonal and in the Lehmann representation,

$$\mathcal{G}_{\mathbf{k}; s, s'}(ip_n) = \delta_{s, s'} \int \frac{d\epsilon}{2\pi} \frac{A_s(\mathbf{k}, \epsilon)}{ip_n - \epsilon + \mu}, \quad (17)$$

where the spectral density $A_s(\mathbf{k}, \epsilon) = \frac{2\Delta_{\mathbf{k}}}{(E^s - \mu)^2 + \Delta_{\mathbf{k}}^2}$ for $s = \pm$ and $\Delta_{\mathbf{k}} = 1/2\tau_{\mathbf{k}}$. Here, $\tau_{\mathbf{k}}$ is the lifetime of the quasiparticle. Using the same techniques developed in Section 8.1 of Mahan's book [48], we obtain the conductivity

$$\sigma = \sum_{s, s'} \int \frac{d^3 \mathbf{k}}{(2\pi)^3} \frac{d\epsilon}{4\pi} J_{\mathbf{k}; s, s'} J_{\mathbf{k}; s', s} A_s(\mathbf{k}, \epsilon) A_{s'}(\mathbf{k}, \epsilon) \delta(\epsilon - \mu). \quad (18)$$

For a large $\tau_{\mathbf{k}}$ (i.e., a small $\Delta_{\mathbf{k}}$), we have $A_s(\mathbf{k}, \epsilon) A_{s'}(\mathbf{k}, \epsilon) \simeq 4\pi \delta(\epsilon - E^s) \tau_{\mathbf{k}}$ when $E^s = E^{s'}$ [48], and $A_s(\mathbf{k}, \epsilon) A_{s'}(\mathbf{k}, \epsilon) = 0$ when $E^s \neq E^{s'}$. Using the fact that $J_{\mathbf{k}} = U_{\mathbf{k}} \overline{\mathcal{J}}_{\mathbf{k}} U_{\mathbf{k}}^\dagger = U_{\mathbf{k}} [\partial_{k_x} (U_{\mathbf{k}}^\dagger \Lambda_{\mathbf{k}} U_{\mathbf{k}})] U_{\mathbf{k}}^\dagger$, we obtain $J_{\mathbf{k}} = U_{\mathbf{k}} (\partial_{k_x} U_{\mathbf{k}}^\dagger) \Lambda_{\mathbf{k}} + \partial_{k_x} \Lambda_{\mathbf{k}} + \Lambda_{\mathbf{k}} (\partial_{k_x} U_{\mathbf{k}}) U_{\mathbf{k}}^\dagger$. Thus, for $E^s = E^{s'}$, we have

$$J_{\mathbf{k}, s, s'} = [U_{\mathbf{k}} (\partial_{k_x} U_{\mathbf{k}}^\dagger) + (\partial_{k_x} U_{\mathbf{k}}) U_{\mathbf{k}}^\dagger]_{s, s'} E_{\mathbf{k}}^{s'} + \delta_{s, s'} \partial_{k_x} E_{\mathbf{k}}^{s'} = \delta_{s, s'} \partial_{k_x} E_{\mathbf{k}}^s. \quad (19)$$

We further assume that $\tau_{\mathbf{k}} = \tau$ and finally obtain

$$\sigma = e^2 \tau \sum_s \int \frac{d^3 \mathbf{k}}{(2\pi)^3} (v_x^s)^2 \delta(E^s - \mu), \quad (20)$$

where $v_x^s = \partial_{k_x} E_{\mathbf{k}}^s$. We have added the factor e^2 , which is preset to be 1 in the derivation above.

Order by order expansion of Eq.(4) in main text

We consider the integral

$$\mathcal{I} = \int_{\text{BZ}} \frac{d^3 \mathbf{k}}{(2\pi)^3} v^2 \delta(E - \mu), \quad (21)$$

where $E(\mathbf{k}, \lambda)$ and $v(\mathbf{k}, \lambda) = E' = \partial_{k_x} E$ are functions of \mathbf{k} and λ . Using the convention $\dot{E} = \partial_\lambda E$, we expand the velocity v and the δ -function around $\lambda = 0$,

$$v^2 \delta(E - \mu) = (v_0 + \dot{v}_0 \lambda + \frac{1}{2} \ddot{v}_0 \lambda^2)^2 (\delta_0 + \dot{\delta}_0 \lambda + \frac{1}{2} \ddot{\delta}_0 \lambda^2), \quad (22)$$

where $v_0 = v|_{\lambda=0}$ and $\delta_0 = \delta(E|_{\lambda=0} - \mu)$. Order by order expanding the function $v^2 \delta(E - \mu)$, we obtain coefficients for λ^i as following,

$$\lambda^0 : \quad v_0^2 \delta_0 \quad (23a)$$

$$\lambda^1 : \quad 2v_0 \dot{v}_0 \delta_0 + v_0^2 \dot{\delta}_0 \quad (23b)$$

$$\lambda^2 : \quad \dot{v}_0 \dot{v}_0 \delta_0 + v_0 \ddot{v}_0 \delta_0 + \frac{1}{2} v_0 v_0 \ddot{\delta}_0 + 2v_0 \dot{v}_0 \dot{\delta}_0. \quad (23c)$$

For simplicity, we will omit the foot index 0 but keep in mind $\lambda \rightarrow 0$. Note that

$$\dot{\delta} = \dot{E} \partial_E \delta = \frac{\dot{E}}{v} \delta', \quad (24)$$

$$\begin{aligned} \ddot{\delta} &= \frac{\partial}{\partial \lambda} (\dot{E} \partial_E \delta) = \ddot{E} \partial_E \delta + \dot{E} \frac{\partial}{\partial \lambda} (\partial_E \delta) = \ddot{E} \partial_E \delta + \dot{E}^2 (\partial_E^2 \delta) \\ &= \frac{\ddot{E}}{v} \delta' + \dot{E}^2 \frac{1}{v} \frac{\partial}{\partial k_x} \left(\frac{1}{v} \delta' \right) = \frac{\ddot{E}}{v} \delta' + \dot{E}^2 \frac{1}{v^2} \delta'' - \dot{E}^2 \frac{v'}{v^3} \delta'. \end{aligned} \quad (25)$$

Integration by parts for the integral (21) shows that these coefficients become

$$\lambda^1 : \quad [(E' \dot{E}' - E'' \dot{E})]_{\lambda=0} \delta(E|_{\lambda=0} - \mu), \quad (26)$$

$$\lambda^2 : \quad \left[\frac{1}{2} \ddot{E}' E' - \dot{E} \dot{E}'' - \frac{1}{2} \ddot{E} E'' + \frac{1}{2} \frac{E'''}{E'} \dot{E}^2 - \frac{1}{2} \frac{E''^2}{E'^2} \dot{E}^2 + \frac{E''}{E'} \dot{E} \dot{E}' \right]_{\lambda=0} \delta(E|_{\lambda=0} - \mu). \quad (27)$$

As a result, we obtain

$$\delta\sigma = e^2 \tau \sum_{\zeta, s} \int_{\text{BZ}} \frac{d^3 \mathbf{k}}{(2\pi)^3} \{ \lambda \mathcal{F}_1[E_\zeta^s] + \lambda^2 \mathcal{F}_2[E_\zeta^s] \} \delta(E_\zeta^s|_{\lambda=0} - \mu), \quad (28)$$

where

$$\mathcal{F}_1[E] = [E' \dot{E}' - E'' \dot{E}]_{\lambda=0}, \quad (29)$$

$$\mathcal{F}_2[E] = \left[\frac{1}{2} \ddot{E}' E' - \dot{E} \dot{E}'' - \frac{1}{2} \ddot{E} E'' + \frac{1}{2} \frac{E'''}{E'} \dot{E}^2 - \frac{1}{2} \frac{E''^2}{E'^2} \dot{E}^2 + \frac{E''}{E'} \dot{E} \dot{E}' \right]_{\lambda=0}. \quad (30)$$

For all models in Table I, the parity symmetry of the functions under $k_x \rightarrow -k_x$, determines that the integral of \mathcal{F}_1 vanishes. The DW resistance becomes

$$R_w = \frac{C_{\text{diffuse}}}{\sigma_0 S} \int_{-L/2}^{L/2} \lambda^2 dx = \frac{2^{\pm 1} C_{\text{diffuse}}}{w \sigma_0 S}, \quad (31)$$

where

$$C_{\text{diffuse}} = -\frac{e^2 \tau}{\sigma_0} \sum_{\zeta, s} \int_{\text{BZ}} \frac{d^3 \mathbf{k}}{(2\pi)^3} \mathcal{F}_2[E_\zeta^s] \delta(E_\zeta^s|_{\lambda=0} - \mu). \quad (32)$$

Here, $2^{\pm 1}$ is for a 180° DW and a 90° DW, respectively. Using $R_0 = L/\sigma_0 S$, we finally obtain $R_w/R_0 = 2^{\pm 1} C_{\text{diffuse}}/Lw$.

When the velocity $v = 0$, the derivative (24) is divergent. The δ -function, as a function of λ , is not differentiable. For this case, if we omit the dependence of δ -function on the spin-spiral parameter λ , then the coefficient for λ^2 in Eq. (23c) becomes $\dot{v}_0 \dot{v}_0 \delta_0 + v_0 \dot{v}_0 \delta_0$, which is fully from the correction of velocity by the spin-spiral. Especially for the A_s model, we use the following approximation to estimate the spin-spiral domain resistance in this case. From Eq.(4) in main text, we have

$$\sigma_\zeta = \frac{e^2 \tau}{2\pi} \sum_s \int dk_x (v_x^{\zeta s})^2 \rho_{\mu - \mathcal{E}_\zeta^s}^{2D}, \quad (33)$$

where

$$\rho_\epsilon^{2D} = \frac{1}{4\pi^2} \int dk_y dk_z \delta(\epsilon - h_2) \quad (34)$$

is the two-dimensional density of state (2D-DOS) for the Hamiltonian $h_2 = -2t(\cos k_y + \cos k_z)$ and \mathcal{E}_ζ^s can be found in Table II. We further treat the 2D-DOS ρ_ϵ^{2D} as a nonzero constant in region $\epsilon \in [-4t, 4t]$ and as zero when $\epsilon \notin [-4t, 4t]$. In this treatment, 2D-DOS of course does not depend on the spin-spiral λ . When the chemical potential $\mu \in [-4t + 2\epsilon_a, 4t - 2\epsilon_a]$, where $\epsilon_a = \sqrt{t^2 + J^2}/4$, the 2D-DOS $\rho_{\mu - \mathcal{E}_\zeta^s}^{2D}$ is nonzero for all k_x in the first Brillouin zone. Thus, $\mathcal{C}_{\text{diffuse}} = -\sum_{\zeta, s} \int_{\text{BZ}} dk_x (\dot{E}'^2 + \ddot{E}' E') / [\sum_{\zeta, s} \int_{\text{BZ}} dk_x E'^2]$, where $E = \mathcal{E}_\zeta^s|_{\lambda=0}$. Finally, We get $\delta\sigma(\lambda)/\sigma_0 = -\mathcal{C}_{\text{diffuse}} \lambda^2 = a^2 \lambda^2 J t^2 / 4\epsilon_a (2t^2 + J^2 - 2\epsilon_a J) > 0$. The spin-spiral enhances the electron mobility and thus the conductivity. For C_s -type, we expect a similar behaviour.

Ballistic transport

For the A_s -type case, we show the classical paths for $\zeta = 1$ in Fig. 4. For the branch \mathcal{E}_ζ^+ , back scattering exists only near $k_x = \frac{\pi}{2}$, where the DW servers as a barrier. It becomes a valley near $k_x = -\frac{\pi}{2}$ and the particles are unobstructed. This can be confirmed by expanding the dispersion \mathcal{E}_ζ^+ around $k_x = \pm \frac{\pi}{2}$ and $\lambda = 0$, showing an effective potential $\pm 2t \sin \frac{\lambda(x)}{2}$. The potential have opposite scattering effects (as barrier or valley) for the branch \mathcal{E}_ζ^- due to the negative effective mass.

Due to the DW, for an effective barrier, open-channel only exists when $|\mathcal{E}_\zeta^s| \in [J_+, 2\epsilon_a]$, where $J_+(\lambda_{\text{max}}) = J + 2t \sin(a\lambda_{\text{max}}/2)$. The conductance (7) in the main text becomes

$$G = \frac{e^2}{2\pi\hbar} S \sum_{i=1}^2 \int_{\mathcal{R}_i} \frac{dk_y dk_z}{4\pi^2}, \quad (35)$$

where $\mathcal{R}_1 = \mathcal{R}(0)$ and $\mathcal{R}_2 = \mathcal{R}(\lambda_{\text{max}})$ with $\mathcal{R}(\lambda) := \{(k_y, k_z) \in \text{BZ} \mid J_+(\lambda) < |\mu - h_2(k_y, k_z)| < 2\epsilon_a\}$. \mathcal{R}_1 represent the effective valley part which contributes no additional resistance from the DW. The increased conductance is $\delta G \simeq -(e^2 S / \pi\hbar) (\rho_{\mu-J}^{2D} + \rho_{\mu+J}^{2D}) \times t \sin(a\lambda_{\text{max}}/2)$. The DW resistance is

$$\frac{R_w}{R_0} = -\frac{\delta G}{G_0} = \mathcal{C}_{A_s} \cdot 2 \sin \frac{a\lambda_{\text{max}}}{2}, \quad (36)$$

where $\mathcal{C}_{A_s}(\mu) = t(\rho_{\mu-J}^{2D} + \rho_{\mu+J}^{2D})/2 \int_{J < |\epsilon - \mu| < 2\epsilon_a} \rho_\epsilon^{2D} d\epsilon$. Now we suppose the 2D-DOS is uniform in the energy region $[-4t, 4t]$. For the case $J \ll 2t$, we obtain

$$\mathcal{C}_{A_s}(\mu) \simeq \begin{cases} t/(6t + \mu), & \mu \in [-4t, -2t], \\ 1/4, & \mu \in [-2t, 2t], \\ t/(6t - \mu), & \mu \in [2t, 4t], \\ 0, & \text{others.} \end{cases} \quad (37)$$

The coefficient $\mathcal{C}_{A_s}(\mu)$ is estimated to be 0.25 to 0.5 for $\mu \in [-4t, 4t]$. For a general J/t , $\mathcal{C}_{A_s}(\mu) = 0$ when $\mu \notin [-4t - J, 4t + J]$, since $\rho_{\mu \pm J}^{2D}$ vanishes outside this region. For moderate filling, using the uniform ρ_ϵ^{2D} , we obtain $\mathcal{C}_{A_s} = t/2(2\epsilon_a - J)$.

Now we consider the A_p type case. k_y and k_z are good quantum numbers, and are fixed during the electron motion. By expanding the spin-spiral dispersion E_ζ^s in Table II as a function of λ , we find that due to the DW, the band width

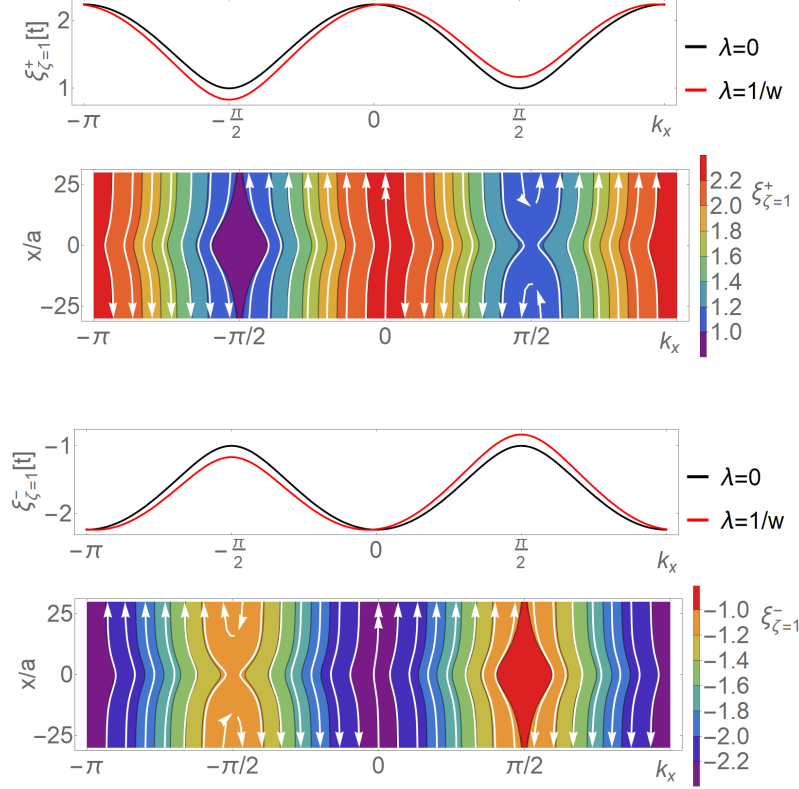


FIG. 4. The color plot of $\xi_{\zeta=1}^{\pm}$ in x - k_x phase space for a 180° DW with $w = 6a$ (for visualization effect, we use this small DW width), and the plot of $\xi_{\zeta=1}^{\pm}$ as functions of k_x for different λ . The lines (with arrow) represent the classical paths in the phase space, which are also the equal-energy contour lines. Here $J = t$.

becomes narrower to $-2t + \lambda_{\max}^2 F_{k_y} + \mathcal{E}^{\pm} < E_{\zeta}^{\pm} < 2t - \lambda_{\max}^2 F_{k_y} + \mathcal{E}^{\pm}$, where $\mathcal{E}^{\pm} = -2t \cos k_x \pm \sqrt{4t^2 \cos^2 k_x + J^2}$ and $F_{k_y} = tJ^2/4(4t^2 \cos^2 k_y + J^2) > 0$. Thus, the conductance (7) in the main text becomes

$$G = \frac{e^2}{\pi h} S \sum_s \int_{\mathcal{R}_s} \frac{dk_x dk_y}{4\pi^2}, \quad (38)$$

where $\mathcal{R}_s := \{(k_x, k_y) \in \text{BZ} \mid \mu - 2t + \lambda_{\max}^2 F_{k_y} < \mathcal{E}^s < \mu + 2t - \lambda_{\max}^2 F_{k_y}\}$. The relative DW resistance has the following form

$$\frac{R_w}{R_0} = \mathcal{D}_{\text{Ap}}(\mu) \cdot a^2 \lambda_{\max}^2. \quad (39)$$

In the following, we estimate the coefficient $\mathcal{D}_{\text{Ap}}(\mu)$ for a moderate filling case. For this purpose, we use the average of F_{k_y} over the first Brillouin zone, $\bar{F}_{k_y} = Jt/8\epsilon_a$, to replace F_{k_y} in the region \mathcal{R}_s . By defining a 2D-DOS $\bar{\rho}_{\epsilon}^s = (1/4\pi^2) \int dk_y dk_z \delta(\epsilon - \mathcal{E}^s)$ for the dispersion \mathcal{E}^s , we obtain the coefficient in terms of 2D-DOS, $\mathcal{D}_{\text{Ap}}(\mu) = \bar{F}_{k_y} [\sum_s (\bar{\rho}_{\mu_+}^s + \bar{\rho}_{\mu_-}^s)] / [\sum_s \int_{\mu_- < \epsilon < \mu_+} \bar{\rho}_{\epsilon}^s d\epsilon]$, where $\mu_{\pm} = \mu \pm 2t$. We further suppose that the total 2D-DOS ($\bar{\rho}_{\mu}^+ + \bar{\rho}_{\mu}^-$) is uniform for $\mu \in [-2t - 2\epsilon_a, 2t + 2\epsilon_a]$, and thus estimate $\mathcal{D}_{\text{Ap}} \sim J/16\epsilon_a$ for a moderate filling case.

Ballistic transport for ferromagnetic metals

It is interesting to compare with ferromagnetic metals with Hamiltonian

$$\mathcal{H}^F = -J\mathbf{n}(x) \cdot \mathbf{s} - 2t(\cos k_x + \cos k_y + \cos k_z)s_0, \quad (40)$$

where \mathbf{n} is the local magnetic moment. We assume that the DW is perpendicular to the x -axis and set $\mathbf{n}(x) = (\sin \theta \cos \phi, \sin \theta \sin \phi, \cos \theta)$, where ϕ is constant and θ depends on x . We also use the replacement $k_x = -i\partial_x$. After the gauge transformation $\mathcal{O}_\theta^F = \mathcal{R}_\theta^F \mathcal{T}^F$, where $\mathcal{R}_\theta^F = \exp[-is_z \phi/2] \exp[-is_y \theta/2]$ and $\mathcal{T}^F = \exp[-is_x \pi/4]$, the Hamiltonian becomes

$$\overline{\mathcal{H}}^F = [\mathcal{O}_\theta^F]^{-1} \mathcal{H}^F \mathcal{O}_\theta^F = -2t \cos(s_z \lambda/2 - is_0 \partial_x) - 2t(\cos k_y + \cos k_z) s_0 - Js_y. \quad (41)$$

where $\lambda = d\theta/dx$.

It has spiral solutions

$$E_{k_x}^\pm = \mathcal{E}_{k_x}^\pm + h_2, \quad (42)$$

where

$$\mathcal{E}_{k_x}^\pm = -2t \cos \frac{\lambda}{2} \cos k_x \pm \sqrt{4t^2 \sin^2 \frac{\lambda}{2} \sin^2 k_x + J^2}, \quad (43)$$

$$h_2 = -2t(\cos k_y + \cos k_z). \quad (44)$$

The band width of $\mathcal{E}_{k_x}^\pm$ is $[-2t \pm J, 2t \pm J]$ at $x = \pm\infty$ where $\lambda = 0$, and becomes narrower to $[-2t \pm J + ta^2 \lambda_{\max}^2/4, 2t \pm J - ta^2 \lambda_{\max}^2/4]$ at $x = 0$ due to the FM-DW. The relative DWMR becomes

$$\frac{R_w}{R_0} = \mathcal{D}_F \frac{a^2}{4 \times 4^d w^2}, \quad (45)$$

where

$$\mathcal{D}_F(\mu) = \frac{t(\rho_{\mu+2t-J}^{2D} + \rho_{\mu+2t+J}^{2D} + \rho_{\mu-2t-J}^{2D} + \rho_{\mu-2t+J}^{2D})}{\int_{-2t-J < |\mu-\epsilon| < 2t-J} \rho_\epsilon^{2D} d\epsilon + \int_{-2t+J < |\mu-\epsilon| < 2t+J} \rho_\epsilon^{2D} d\epsilon}, \quad (46)$$

and ρ_ϵ^{2D} is defined by Eq. (34). We estimate $\mathcal{D}_F(E_F) \sim 0.5$ for a moderate filling case by assuming a uniform 2D-DOS. For low filling case, $\cos k \simeq 1 - k^2/2$, the new scale k_F^2 appears, and we find $\mathcal{D}_F(\mu) = 1/k_F^2$ for small J/t (two bands are occupied). It recovers the previous result [32, 33].

Fig. 5: Plot of diffuse conductivity $\sigma(\lambda)$ and DOS

Fig. 6: Plot of ballistic conductance G_0

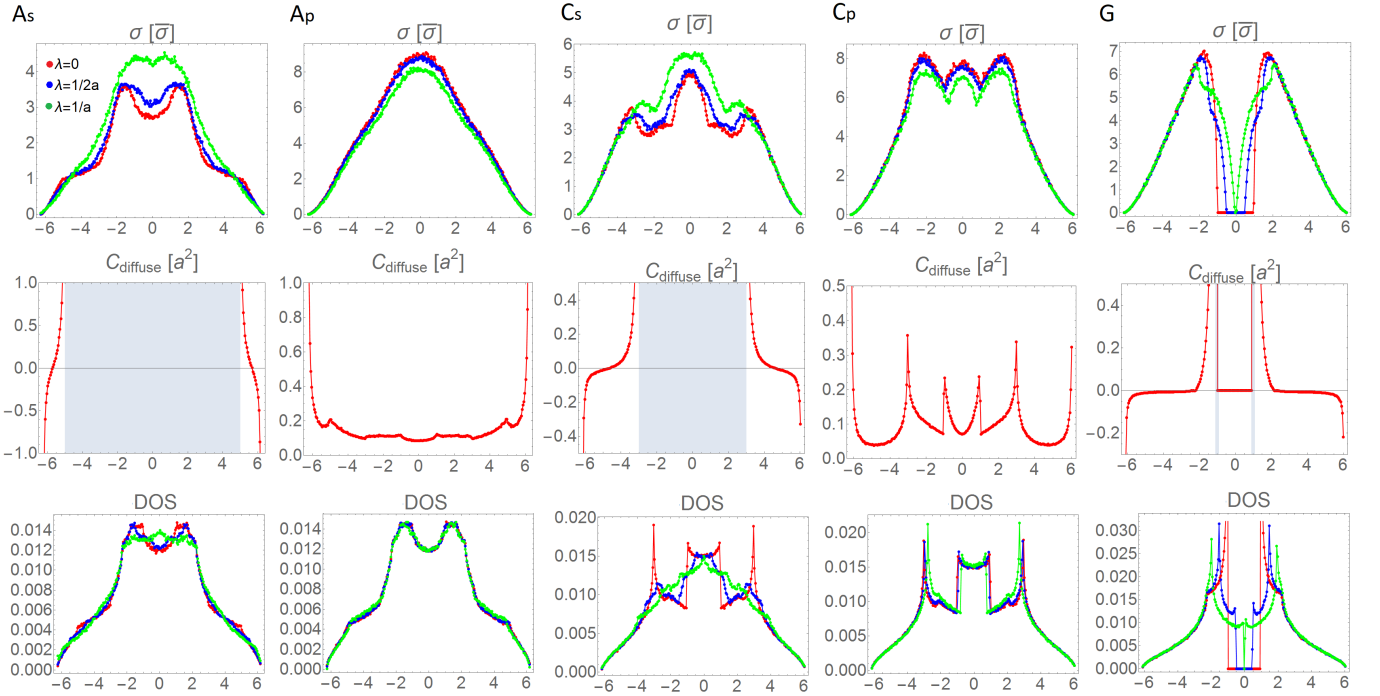


FIG. 5. Diffuse conductivity $\sigma(\lambda)$, the coefficient C_{diffuse} and DOS as functions of the chemical potential μ (in unit $[t]$) for different models. For visualization the difference in different spin-spiral cases, we chose a large exchange interaction, $J = t$. The unit $\bar{\sigma} = e^2\tau/3\pi^2m_0a^3$, where $m_0 = 1/2t$.

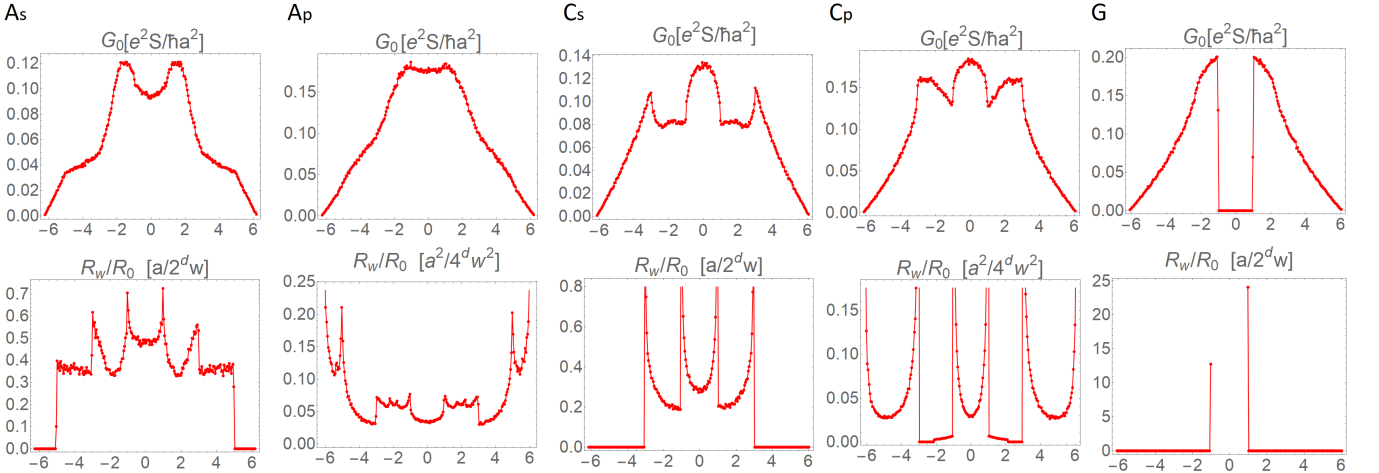


FIG. 6. Ballistic conductance G_0 and R_w/R_0 as functions of the chemical potential $\mu[t]$ for different models. Here, $J = t$.